MaGICC Halos: Confronting Simulations with Observations of the Circum-Galactic Medium at z=0

G. S. Stinson[1]⋆, C. Brook [2,3], J. Xavier Prochaska[4,1], Joe Hennawi[1], Andrew Pontzen[5], Sijing Shen[4], J. Wadsley[6], H. M. P. Couchman[5], T. Quinn[7], Andrea V. Macciò[1], Brad K. Gibson[2,8]

[1] *Max-Planck-Institut für Astronomie, Königstuhl 17, 69117, Heidelberg, Germany*
[2] *Jeremiah Horrocks Institute, University of Central Lancashire, Preston PR1 2HE*
[3] *Departamento de Física Teórica, Universidad Autónoma de Madrid, E-28049 Cantoblanco, Madrid, Spain*
[4] *Department of Astronomy & Astrophysics, UCO/Lick Observatory, University of California, 1156 High St, Santa Cruz, CA 95064*
[5] *Astrophysics, University of Oxford, Denys Wilkinson Building, Keble Road, Oxford OX13RH*
[6] *Department of Physics and Astronomy, McMaster University, Hamilton, Ontario, L8S 4M1, Canada*
[7] *Astronomy Department, University of Washington, Box 351580, Seattle, WA, 98195-1580*
[8] *Department of Astronomy & Physics, Saint Mary's University, Halifax, Nova Scotia, B3H 3C3, Canada*

24 April 2018

ABSTRACT

We explore the circumgalactic medium (CGM) of two simulated star-forming galaxies with luminosities $L \approx 0.1$ and $1L^\star$ generated using the smooth particle hydrodynamic code GASOLINE. These simulations are part of the Making Galaxies In a Cosmological Context (MaGICC) program in which the stellar feedback is tuned to match the stellar mass–halo mass relationship. For comparison, each galaxy was also simulated using a "lower feedback" (LF) model which has strength comparable to other implementations in the literature. The "MaGICC feedback" (MF) model has a higher incidence of massive stars and an $\approx 2\times$ higher energy input per supernova. Aside from the low mass halo using LF, each galaxy exhibits a metal-enriched CGM that extends to approximately the virial radius. A significant fraction of this gas has been heated in supernova explosions in the disk and subsequently ejected into the CGM where it is predicted to give rise to substantial OVI absorption. The simulations do not yet address the question of what happens to the OVI when the galaxies stop forming stars. Our models also predict a reservoir of cool HI clouds that show strong Lyα absorption to several hundred kpc. Comparing these models to recent surveys with the *Hubble Space Telescope*, we find that only the MF models have sufficient OVI and HI gas in the CGM to reproduce the observed distributions. In separate analyses, these same MF models also show better agreement with other galaxy observables (e.g. rotation curves, surface brightness profiles, and HI gas distribution). We infer that the CGM is the dominant reservoir of baryons for galaxy halos.

1 INTRODUCTION

In the paradigm of cold dark matter (CDM) cosmology, gravitational collapse leads to the formation of virialized and bound dark matter halos. It is predicted that baryons fall into these halos with the dark matter, comprising a mass fraction up to the cosmological ratio. Recent analyses indicates that stars comprise less than 25% of the baryons that should have collapsed into halos (Conroy & Wechsler 2009; Mandelbaum et al. 2009; Moster et al. 2010; Guo et al. 2010; More et al. 2011). This presents a "missing baryon" problem reflected in the unknown whereabouts of the baryons, which did not cool to form stars. Substantial amounts of gas are found in a diffuse and highly ionized medium which is referred to as halo gas or the circumgalactic medium (CGM).

The CGM is known to manifest in at least two phases: (i) a warm/hot, collisionally ionized gas with temperature near the virial temperature ($T > \sim 10^6$ K); and (ii) a cooler phase (perhaps predominantly photoionized) with temperature $T \lesssim 10^4$ K. The latter phase has been detected in 21cm emission in our Galaxy in the population known as the high velocity clouds (e.g. Wakker & van Woerden 1997) lying at distances of tens of kpc (Thom et al. 2006). The hotter phase may be observed via bremsstrahlung emission with X-ray telescopes, in the intracluster medium of massive galaxy clusters (e.g. Allen et al. 2001), but so far extended diffuse emission has only been detected around one disc galaxy, the massive NGC1961 (Anderson & Bregman 2011). Smaller disc galaxies have X-ray bright outflows

(Strickland et al. 2004), but halo emission remains undetected.

The diffuse nature of the CGM makes positive detections of emission rare. The majority of empirical constraints, therefore, come from absorption-line analysis of galactic halos, along coincident sightlines to distant quasars and galaxies (e.g. Bowen et al. 1996; Lanzetta et al. 1995; Chen & Tinker 2008; Rubin et al. 2010; Steidel et al. 2010). These observations reveal a cool and frequently metal-enriched phase traced by HI Lyman series absorption (e.g. Chen & Lanzetta 2003) and low-ionization metal-line transitions (e.g. Chen & Tinker 2008; Barton & Cooke 2009; Rubin et al. 2012). Importantly, galaxies of essentially all luminosity and spectral type exhibit significant HI absorption out to impact parameters $R \approx 300\,\mathrm{kpc}$ (Wakker & Savage 2009; Prochaska et al. 2011), implying a massive ($M \sim 10^{10} M_\odot$) extended CGM.

A particularly useful tracer of the hot phase in quasar absorption line analysis is the OVI doublet, which occurs in highly ionized and enriched regions of the Universe. If collisionally ionized, the gas has temperature $T \sim 10^5 - 10^6$ K. OVI is observed along the majority of sightlines through our Galactic halo and is believed to trace coronal material on scales of 10–100kpc (Sembach et al. 2003). This gas is also associated with the CGM of local $L > 0.1L^\star$ galaxies (Stocke et al. 2006; Wakker & Savage 2009). Prochaska et al. (2011) have further demonstrated that the extended CGM ($R \sim 300\,\mathrm{kpc}$) of $L > \sim 0.1L^\star$ galaxies has a high covering fraction to OVI and can account for all of the OVI detected in the present-day universe. Most recently, Tumlinson et al. (2011) report a nearly 100% incidence of strong OVI absorption for the halos of $L \sim L^\star$ star-forming galaxies, with an ionized metal mass that likely exceeds that of the galaxies' interstellar media, demonstrating that the CGM is a major reservoir of highly ionized metals at $z \sim 0$.

The observations reveal a multi-phase, highly ionized and metal-enriched CGM around present-day galaxies (also see Thom & Chen 2008b; Savage et al. 011a,b; Wakker et al. 2012). The high degree of enrichment demands that a large mass of gas (and metals) is transported from galaxies and/or their progenitors to the CGM. Thus, these observations provide robust constraints on the processes of gas accretion and feedback which may be compared directly against models of galaxy formation.

Previous theoretical work on the CGM for individual galaxies has largely focused on analytic or semi-analytic treatments of idealized gas and dark matter/temperature profiles (Mo & Miralda-Escude 1996; Telfer et al. 2002; Maller & Bullock 2004; Binney et al. 2009). Although these works provide crucial insight into the nature of the CGM, they lack proper cosmological context (e.g. mergers) and have generally not included the role of feedback from star-formation in the galaxy and its satellites. The latter is now considered critical to match a wide-range of galaxy observables including the luminosity function, the stellar mass–halo mass relationship, and the baryonic Tully–Fisher relationship (Guo et al. 2011). Galactic-scale winds likely resulting from stellar feedback are a nearly generic feature of star forming galaxies (Shapley et al. 2003; Weiner et al. 2009; Rubin et al. 2010) and may significantly influence properties of the CGM.

A number of groups have now used cosmological simulations to examine the nature and enrichment of the IGM at $z \sim 0$ and offer comparisons to quasar absorption line observations (e.g. Cen & Ostriker 2006; Davé et al. 2010; Oppenheimer et al. 2012; Smith et al. 2011; Cen 2012). These studies have not explicitly examined the physical nature of the CGM for individual galaxies and likely have insufficient resolution to perform such analysis. A few authors have examined the distribution of gas within individual galactic halos, but have not yet treated the distribution of metals or the impact of feedback (Kereš & Hernquist 2009; Stewart et al. 2011). At $z \sim 3$, Kawata & Rauch (2007) have analyzed numerical simulations of outflows in L* progenitors, and found that OVI better reflects the strength of galactic winds than HI. Most recently, Fumagalli et al. (2012) and Shen et al. (2011) have examined the metal enrichment of the CGM with the latter demonstrating that metals can be ejected to large distances at early times from L* progenitor galaxies while their gravitational potential remains low.

We have recently begun the MaGICC project to use sufficient stellar feedback to simulate galaxies that match the stellar mass–halo mass relationship. Early results of the project have shown that the ejection of low angular momentum gas via outflows (Brook et al. 2011) redistributes angular momentum via large scale galactic fountains (Brook et al. 2012) and thus play a crucial role in forming disc galaxies, particularly those without classical bulges. In this way, we form galaxies that match scaling relations between rotation velocity, size, luminosity, colour, stellar mass, halo mass, HI mass, baryonic mass and metallicity (Brook et al. 2012, submitted). Macciò et al. (2012) also showed that these galaxies have cored dark matter density profiles. Here, we test the baryon cycle of these simulations with the constraints provided by observations of the CGM, and in particular the column densities of H I and O VI as observed at $z = 0$.

2   SIMULATIONS

We resimulate a suite of simulations drawn from the McMaster Unbiased Galaxy Simulations (MUGS, Stinson et al. 2010). The simulations are listed in Table 1. The highest mass galaxy, HM, is g5664 from MUGS and is about half the Milky Way's halo mass. The low mass galaxies, LM_MF and LM_LF, are rescaled versions of MUGS initial conditions, each a factor of eight lower mass than the MUGS simulations, allowing us to explore mass dependence. LM_MF was also used in Brook et al. (2012).

The simulations were evolved using the smoothed particle hydrodynamics (SPH) code GASOLINE (Wadsley et al. 2004). Supernova energy is implemented using the blastwave formalism (Stinson et al. 2006). Metals are ejected from type II supernovae (SNII), type Ia supernovae (SNIa), and the stellar winds of asymptotic giant branch (AGB) stars. Ejected mass and metals are distributed to the nearest neighbour gas particles using the smoothing kernel (Stinson et al. 2006). Metal diffusion is included and metal cooling is calculated based on the diffused metals (Shen et al. 2010).

Two different star formation and feedback models are

Table 1. Simulation data

Name	$M_{tot}{}^a$ (M$_\odot$)	$M_\star{}^b$ (M$_\odot$)	Luminosity^c (L*)	c$\star^d$	$\epsilon_{rp}{}^e$
HM_MF	7×10^{11}	1.4×10^{10}	0.84	0.1	0.175
HM_LF	7×10^{11}	4.8×10^{10}	0.79	0.05	–
LM_MF	1.8×10^{11}	3.7×10^{9}	0.15	0.05	0.1
LM_LF	8.8×10^{10}	8.7×10^{9}	0.13	0.05	–

^{a} M_{tot} is the virial mass of the halo including dark and baryonic matter.
^{b} $M_\star$ is the total stellar mass.
^{c} V-band luminosity compared to $M_V = -21$.
^{d} Star forming efficiency.
^{e} Radiation Pressure Efficiency.
^{f} Initial Mass Function: C=Chabrier (2003); K=Kroupa et al. (1993)

employed. The original MUGS simulations formed stars when gas reached a density of 1.0 cm^{-3}, used a Kroupa et al. (1993) IMF and deposited 0.4×10^{51} ergs per supernova explosion. We refer to this as the "lower feedback model" (LF) in this study, but note that this feedback strength is comparable to or even stronger than most implementations that are currently run in the literature (Scannapieco et al. 2012). In our "MaGICC feedback model" (MF), four changes have been made to our implementation of star formation and feedback:

• we use the more common Chabrier (2003) IMF which creates more massive stars for a given stellar mass;
• the star formation density threshold is increased to 9.3 cm^{-3};
• the energy input from supernovae is increased to 10^{51} ergs;
• we include energy from radiation released by the massive young stars before they explode as supernovae.

Radiation pressure from massive stars can have significant effects on the scales that are resolved in our simulations (Nath & Silk 2009; Murray et al. 2011). Massive stars typically produce 10^{50} ergs of energy per $M_\odot$, yet this couples only weakly to the ISM (Freyer et al. 2006). To mimic this inefficiency, we inject a fraction of the energy as thermal energy in the surrounding gas but do *not* turn off cooling (for details see Brook et al. 2012). Such thermal energy injection is highly inefficient at the spatial and temporal resolution of cosmological simulations, and is rapidly radiated away (Katz 1992) This feedback is even less efficient at low resolution. Following a parameter search designed to match the stellar mass–halo mass resolution from halo abundance matching (Moster et al. 2010), we inject 17.5% of radiation pressure to the surrounding gas as thermal energy in the lower resolution (HM) simulation, but only 10% in the higher resolution runs(LM). The overall coupling of energy to the ISM is minimal, but sufficient to reduce star formation in the region immediately surrounding a recently formed star particle.

The HM_LF and HM_MF simulations use the same initial conditions and each simulated galaxy has an absolute V-band magnitude $M_V \approx -20.8$ implying a luminosity $L \approx 0.8L^\star$. This is somewhat surprising given that the two runs yield very different stellar masses for the galaxy;
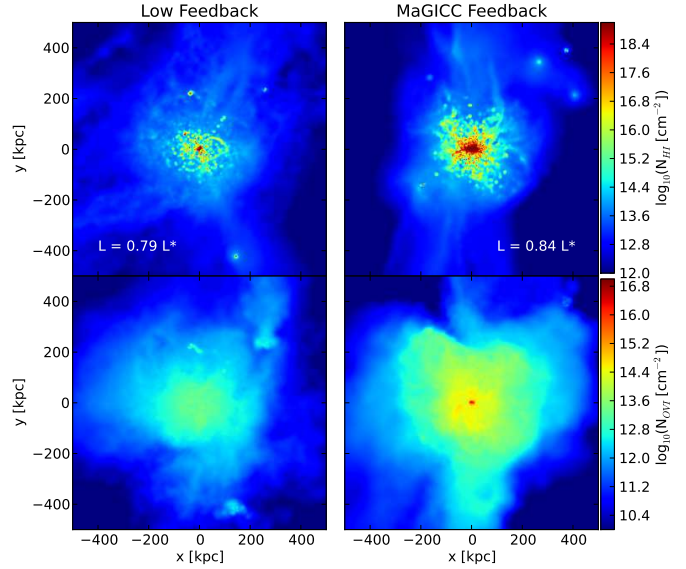

Figure 1. Column density maps of HI (*top*) and OVI (*bottom*) of the low (*left*) and high (*right*) feedback simulations. The maps are all aligned so that the discs of the galaxies are edge on to the viewer. The results on scales greater than 10 kpc are relatively independent of viewing angle.

this difference is compensated by the fact that each galaxy follows a very different star formation history (see Figure 7) such that the different stellar ages result in comparable V-band luminosity, but $B - V$ colours of 0.37 for HM_MF and 0.55 for HM_LF. HM_MF was analysed in Macciò et al. (2012). LM_LF and LM_MF use different initial conditions of similar halo mass. They are selected because each has $M_V \approx -19$. The LM_LF initial conditions run with MaGICC feedback have $M_V \approx -16.2$. To summarize the internal properties of the galaxies, the lower feedback galaxies suffer from the problems of angular momentum loss that have long plagued galaxy formation simulations: dense central stellar bulges, centrally peaked rotation curves, dark matter cusps and too many stars relative to halo mass compared to observations. The MaGICC feedback simulations result in galaxies which match the stellar mass–halo mass relation, have slowly rising rotation curves, and dark matter cores. The MaGICC feedback simulations provide significantly better matches to the internal properties of observed disc galaxies.

3 RESULTS

To study the CGM properties of the simulated galaxies, we find the galaxy using the Amiga Halo Finder (Knollmann & Knebe 2009) and define its center and systemic velocity by the position and velocity of the particle with the lowest potential. We may then sample the CGM at a range of impact parameters ρ. To generate surface density maps of the CGM, we sum each box over 1 Mpc along the line of sight. The maximum velocity of the material in the box is $|\delta v| < 200\,\mathrm{km\,s^{-1}}$. To estimate the specific column densities of HI and OVI, we must estimate the ionization state of the gas along each sightline. Under equilibrium conditions, which we assume apply, the ionization state is
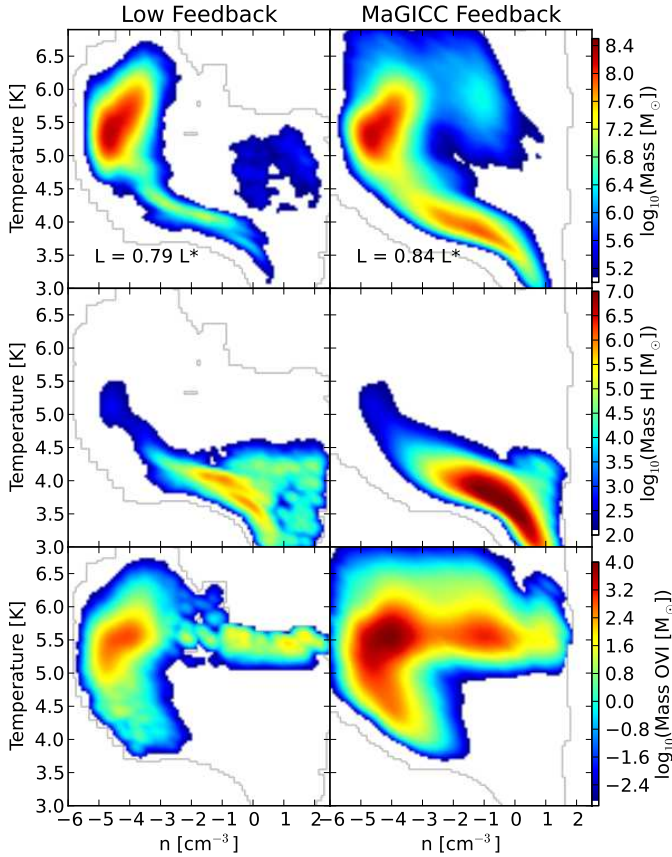
Figure 2. Temperature-density phase diagrams of the galaxy halo simulated with the two different amounts of feedback. The top plots are mass weighted by the total gas mass, the middle is weighted by the HI mass, and the bottom is weighted by O VI. These phase diagrams only include halo gas, that is gas more than 3 kpc above or below the midplane or at $R_{xy} > 40$ kpc. The distinct locations of OVI and HI show that the hot and cold gas is in different phases in our model.

determined by the incident radiation field (photoionization) and temperature of the gas (collisional ionization). A proper handling of radiative transfer effects are beyond the scope of this present paper. Instead, we examine the simulations in regions expected to correspond to optically thin material, i.e. where the HI column density is low because the gas is expected to be highly ionized.

We calculated the ionization states for hydrogen and oxygen throughout the high resolution region assuming optically thin conditions and the Haardt & Madau (2012) UV radiation field evaluated at $z = 0$. With the Cloudy software package (v10.0 last described in Ferland et al. (1998)), we generated a suite of models varying the density, temperature, and metallicity of the medium and used the output to find the OVI and HI fractions for all the gas in the simulation.

In Figure 1 we present column density maps for HI and OVI for the LF and MF runs of galaxy HM. Both simulations predict a CGM extending to at least 100 kpc traced by cool HI gas and the more highly ionized OVI gas. Figure 2 presents three phase-diagrams of the CGM material
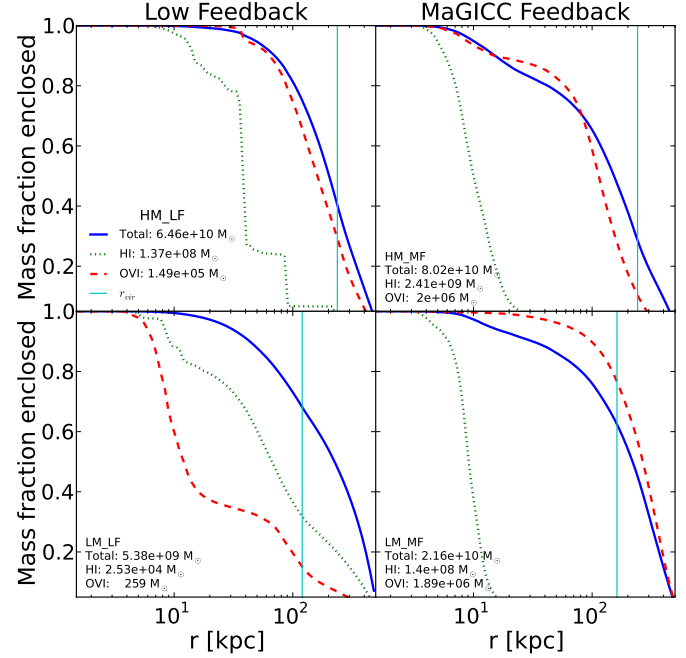

Figure 3. Cumulative gas mass profiles from 500 kpc inwards for each of the 4 galaxies. The solid line represents total gas mass, the dashed line represents OVI, and the dotted line represent HI. The total mass of each component is given in the legend of each plot. With the MaGICC feedback, the HI has a more centrally concentrated profile than the OVI. In the $\sim L^{\star}$ galaxy, HM_MF, the OVI distribution follows the total gas distribution fairly closely, but in the lower mass galaxy, the OVI is significantly more extended than the total gas, indicating that enriched material is blown farther away.

in each galaxy. The top phase diagrams include the total halo gas mass in the simulations. The middle only counts HI mass and the bottom only counts the mass of the halo OVI. One notes two distinct phases in the top panels: (i) a cool ($T \sim 10^4$K), dense ($n > 10^{-2}$ cm^{-3}) gas which dominates the HI absorption and (ii) a warm/hot ($T > 10^5$K) gas, which the bottom panels show creates the OVI, primarily through collisional ionization.

The MaGICC Feedback simulation shows a high density hot component, which seems unphysical that accounts for 9% of the halo OVI at $z = 0$. We find that 90% of this high density, hot halo gas is a relic of the thermal feedback implementation–the gas has had its cooling temporarily disabled–and that this gas is concentrated in a $\sim$10 kpc sphere around the galaxy. This dense, hot gas drives the outflows that populate the CGM with metal enriched material, but it represents a negligible fraction of the OVI column. We discuss in §3.3 how this dense, hot gas generates a comparable amount of soft X-ray emission to that observed.

In terms of total mass, Figure 3 shows that the CGM of the HM_MF galaxy has $4 \times 10^{10}\, M_{\odot}$ ($7 \times 10^{10}\, M_{\odot}$) of gas to $\rho = 150(300)$ kpc. (We quote 300 kpc since it is the maximum extent at which OVI maintains a 100% covering fraction in the simulations.) About half of this CGM has $T < 10^5$ K giving a cool gas mass that matches very well with previous empirical estimates (Prochaska et al. 2011). Regarding metals, the CGM has $\sim 10^6 M_{\odot}$ of OVI to

$R = 150$ kpc, again in excellent agreement with the mass estimates for $L \approx L^\star$, star-forming galaxies (Tumlinson et al. 2011). The LM_MF model has a lower CGM mass in both gas and metals by about a factor of 3. The LM_LF has even less ($\sim 10^9 M_\odot$) cool gas in the CGM and a negligible mass of OVI. This model is a very poor match to the observational estimates.

Returning to Figure 1, one notes that the OVI gas has both a smoother and more extended distribution than the HI. Again, this reflects the fact that the OVI gas traces a hotter and more diffuse phase in the halos of this galaxy. In contrast, the discrete clouds of HI are clustered more closely to the disc and are the remnant of both gas-rich mergers and cooling out of the hot halo. Maller & Bullock (2004) and Kaufmann et al. (2009) describe how gas can cool out of the hot halo. A detailed examination of the evolution of these cold clouds is beyond the scope of this paper, but a preliminary investigation suggests that the clouds both cool out of the hot halo and are entrained in the outflows. The cooling mechanism may be a numerical artifact of SPH whereby particles approach each other due to random excursions and thus create a slightly higher density, which makes them cool faster. Fewer condensations are seen using hydrodynamics based on the Eulerian (grid) method (Teyssier 2002; Agertz et al. 2011) or the new moving mesh code AREPO (Springel 2010; Vogelsberger et al. 2011). It remains for future simulations using more detailed radiative transfer to see if such condensations are an artifact of the SPH hydrodynamics scheme.

In Figure 4, we present the surface density profiles of HI gas and in Figure 5 we present the surface density profiles of OVI gas as a function of the impact parameter ρ to the center of the galaxy. Overplotted on the distributions are observed HI and OVI column densities for sub-$L^\star$ galaxies at $z \sim 0$ from Prochaska et al. (2011) and for star-forming $L^\star$ galaxies at $z \sim 0.2$ from Tumlinson et al. (2011). We also mark each panel with the V-band luminosity of the simulated galaxies and the virial radius, indicated by the vertical green line. Considering first the lower feedback HM_LF, we find fair agreement for the HI gas although the data are systematically higher than the majority of simulated sightlines. The results for OVI are more discordant; the CGM of HM_LF underpredicts the observed OVI column densities by nearly an order of magnitude at all impact parameters. In contrast, the HM_MF predicts nearly $10\times$ higher OVI surface densities and therefore provides a reasonable match to the observations. Furthermore, this model yields qualitatively better agreement with the HI observations. In these respects, this single simulation of an $L \approx 0.8L^\star$ galaxy has a CGM with characteristics matching current observations. At lower masses, the differences between the high and lower feedback models become starker. LM_LF has an undetectable OVI content beyond the optical extent of the galaxy even though the data for galaxies of comparable luminosity all show detections of OVI. In contrast, LM_MF predicts a factor of 10^4 higher OVI surface densities, matching observations.

3.1 Halo Oxygen Distribution Function

Figure 6 shows the oxygen distribution function of the halo gas in the four simulations. The MaGICC feedback cases
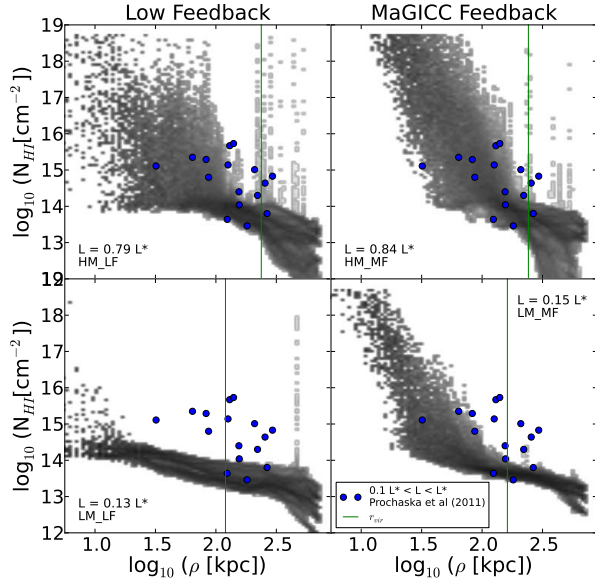

Figure 4. Radial profiles of the column density maps of HI for the four simulated galaxies. Large blue dots are observations of $0.1 L^\star < L < L^\star$ from the Prochaska et al. (2011) galaxy sample while large green squares are galaxies with $L < 0.1L^\star$. The solid green line represents the virial radius, r_{vir}, for each of the four halos.

result in a broad distribution of oxygen abundance with a peak at half the solar oxygen abundance comparable to the abundances measured in Milky Way halo gas (Gibson et al. 2000, 2001). The Lower Feedback simulations are at least 2 orders of magnitude less oxygen enriched. In total, HM_MF has 1.2×10^8 $M_\odot$ of oxygen in its halo, roughly twice the 7.7×10^7 $M_\odot$ of oxygen contained in the ISM in the disk, while LM_MF has roughly an equipartition between the 1.6×10^7 $M_\odot$ in its halo and 2.1×10^7 $M_\odot$ in its disk (cf Tumlinson et al. 2011). Lower feedback generates gaseous halos with significantly less oxygen.

3.2 Evolution

To gain a sense of how the CGM developed, Figure 7 shows the evolution of total mass, along with stellar, OVI, cold ($T < 10^5$ K), and hot gas ($T > 10^5$ K) masses within r_{vir} for the simulated galaxies. The total halo mass increases by two orders of magnitude in the 2 Gyr between $z = 6$ and 3 in each simulation. Subsequent merger/accretion events are reflected in mass "jumps". With lower feedback, most star formation happens early, at the same time the total mass is rapidly increasing. High feedback delays this star formation.

In each galaxy, hot gas develops at the same time as star formation, indicating that stellar feedback is the initial source of hot gas in galaxy halos. As the halo grows, accreting cold gas is shocked to the virial temperature, so that by $z = 0$, only one-third of $T > 10^5$ K gas at $z = 0$ was directly involved in a stellar feedback event. The mass history of the OVI follows stellar mass in HM_MF indicating that oxygen produced in supernovae readily makes its way into the halo as a hot gas. In HM_LF, the OVI mass initially rises, but then drops during its major merger at $z = 1.5$ after which
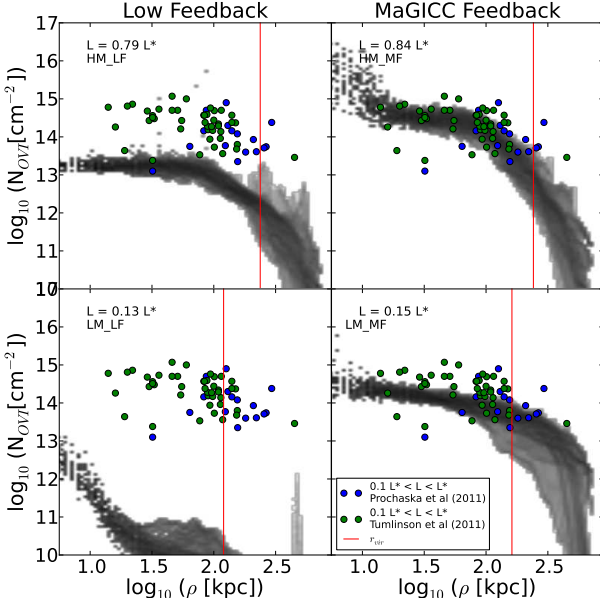
Figure 5. Radial profiles of the column density maps of OVI for four galaxies spanning a range of masses simulated using MaGICC feedback simulations. The large dots are observations of 0.1 L_*<L<L galaxies from the Prochaska et al. (2011) (*blue*) and Tumlinson et al. (2011) (*green*) galaxy samples. The solid red line represents the virial radius, r_{vir}, for each of the four halos.
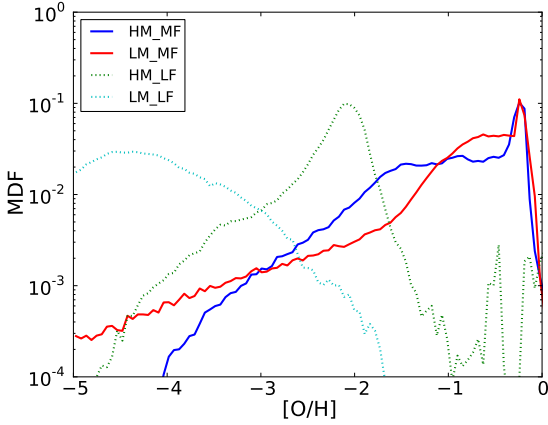

Figure 6. The oxygen distribution function for the four galaxies in our sample. The MaGICC feedback produces a significantly metal-enriched gas halo with a peak in both the HM and LM galaxy just above half solar.

the OVI mass remains constant indicating that the lower feedback is unable to drive metal-enriched outflows.

It is surprising that even though the feedback implementation is thermal, the MaGICC feedback does not lead to more hot gas, but rather more cold gas. As described earlier, this is because some cold gas gets entrained in outflows and there is rapid cooling of halo gas. We speculate that the similar amount of hot gas in HM_LF and HM_MF that have different feedback implementations is representative of some maximum amount of hot gas that can exist in a halo before the gas cools; a larger parameter search is required to address this question.
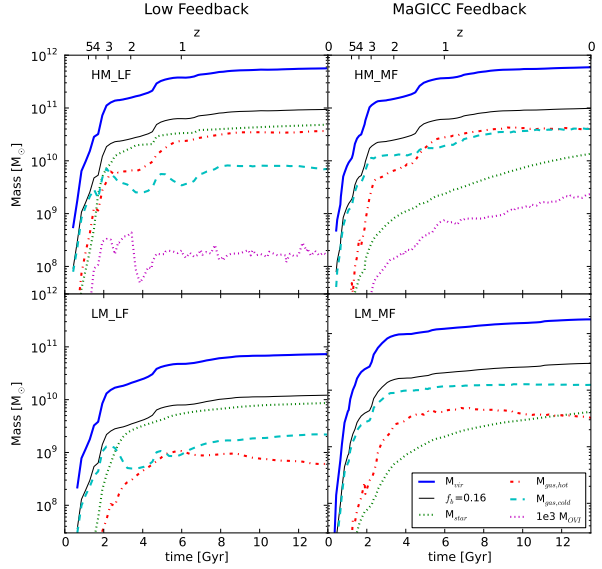

Figure 7. The mass evolution of the total halo mass (*blue*), stellar mass (*dotted-green*), $10^3 \times$OVI mass (*dotted-magenta*), total gas (*dashed light blue*), and hot (T> 10^5 K) gas within r_{vir} for the 4 simulations. The thin black line shows the cosmic baryon fraction of the total halo mass.

3.3 X-ray Emission

One consequence of predicting that the OVI comes from a massive halo of collisionally excited gas ranging up to 10^7 K is that it should produce diffuse soft (0.2-2.0 keV) X-ray emission. Observations of disc galaxies have detected X-rays from outflows less than 10 kpc from the disc, but never $L_X > 5.2 \times 10^{39}$ erg s^{-1} outside 10 kpc (Strickland et al. 2004; Anderson & Bregman 2011). Using a naive Navarro et al. (1995) estimate of L_X based solely on bremsstrahlung cooling, HM_MF has $L_X = 5.2 \times 10^{39}$ (4.4×10^{37}) erg s^{-1} outside 10 (20) kpc in the 0.2-2.0 keV energy range. Even with the large amount of mass in the halo, the gas remains too diffuse to emit significant X-rays. It is intriguing that the X-ray luminosity from inside 10 kpc, $L_X = 5.8 \times 10^{40}$, is similar to the observed diffuse, soft X-ray emission for an $L_B = 2.4 \times 10^{10}$ L$_\odot$ galaxy (e.g. Strickland et al. 2004), but a detailed study of this emission is beyond the scope of this work.

4 CONCLUSIONS

We have studied CGM gas in high resolution galaxy formation simulations. The stellar feedback is constrained using the stellar mass–halo mass relationship. This constraint leads to a stellar feedback implementation that decreases star formation and ejects hot, metal-enriched gas into the CGM. Inside the galaxies, the stellar feedback results in slowly rising rotation curves, flattened dark matter density profiles and HI mass-Luminosity, baryonic Tully–Fisher relations, and mass-metallicity relations that resemble observed galaxies (Brook et al. 2012). We compared these galaxy models to one with more standard feedback implementation (Stinson et al. 2010; Scannapieco et al. 2012). The lower

feedback simulations match none of these commonly observed internal properties of galaxies. An examination of the CGM in our model reveals that:

• The MaGICC feedback implementation produces extended, metal-enriched gaseous coronae that extend to impact parameters of ∼300 kpc, even around low mass ($L_* \sim 0.1 L_\odot$) halos. These results match observed absorption line features (Wakker & Savage 2009; Prochaska et al. 2011; Tumlinson et al. 2011).

• The hot coronae extend beyond r_{vir}, though most of their mass remains contained within r_{vir} of the simulated galaxies. The coronae extend furthest outside r_{vir} in low mass systems.

• A reasonably strong feedback implementation, compared with those in the literature (our "lower feedback" case), is insufficient to match HI absorption features at $z = 0$ and severely underestimates OVI, performing particularly poorly in low mass ($\sim 0.1\ L^\star$) simulations.

• The amount of hot gas in the LF and MF runs did not differ significantly, but rather:

– (i) The MaGICC feedback ejected ten times more oxygen out of the disc than the lower feedback in the high mass case and a factor of 10^4 more in the low mass case.

– (ii) The MaGICC feedback halo contains ten times the cold gas as the lower feedback case in both high and low mass simulations. The cold gas results from cooling out of the hot halo gas and cold gas entrained in outflows.

• The MaGICC feedback simulations match the observed HI and OVI absorption columns at a range of masses.

• The total mass of the coronae is several times higher than the stellar mass in the simulated MaGICC feedback galaxies. Thus, the simulations of individual galaxies predict that the "missing baryons" are found in the CGM of galaxies.

In our simulations, we only considered galaxies defined as star forming by Prochaska et al. (2011) and Tumlinson et al. (2011). One of the key results of those works is the absence of OVI detection in quiescent galaxies. Our simulations are unable to address the question of what happens to the OVI when galaxies stop forming stars.

Our examination focused on the radial distribution of HI and OVI gas in the CGM of a simulated $L \approx L^\star$ galaxy and compared these results to observed surface density profiles. There are, of course, additional observables related to the entire population of OVI absorbers identified in quasar absorption line studies (e.g. Danforth & Shull 2008; Thom & Chen 2008a; Tripp et al. 2008); any truly successful model must also reproduce these resuts. One key constraint is the observed distribution of line-widths (a.k.a. Doppler parameters or b-values) for the OVI gas (Thom & Chen 2008a; Tripp et al. 2008) which gauge, in a statistical fashion, the contributions of thermal broadening, turbulence, and gas dynamics to the motions of the gas. On average, the b-values for OVI absorbers are substantial ($b > 20 \mathrm{km\ s^{-1}}$) and appear to correlate with the strength of OVI absorption. This has posed a considerable challenge to models where OVI is predominantly photoionized (e.g. Oppenheimer & Davé 2009), as such gas has a small thermal width. Another valuable kinematic constraint is the common observation of co-aligned HI and OVI absorption relative

to a common redshift (approximately half of observed OVI systems; Thom & Chen 2008b). Indeed, this appears to be at odds with the apparent separation of strong HI absorption (at smaller radii) with the extended OVI absorption of our modeled CGM. On the other hand, we do observe non-negligible HI absorption to large radii (Figure 4) which may trace the OVI gas. A proper comparison of our model with these observables will require the generation and detailed analysis of line-profiles, as well as the examination of the CGM for galaxies spanning a wide range of masses. This will be the focus of our next paper, which will consider whether the extended CGM of $z \sim 0$ galaxies can reproduce all of the observed statistics for OVI as argued by Prochaska et al. (2011).

We further note that the HI surface densities at $\rho < 50\,\mathrm{kpc}$ are sufficiently large that the CGM will yield significant absorption from lower ionization states of heavy metals (e.g. MgII, SiII, SiIII). A proper estimate of the column densities for these ions, however, will require a full treatment of radiative transfer (i.e. to account for self-shielding by optically thick HI gas).

The fact that the resultant extended, metal enriched CGM around our simulated galaxies matches the observations over a wide range of mass provides strong support for a vigorous baryon cycle in which outflows and subsequent cooling of halo gas play a key role in forming disc galaxies.

REFERENCES

Agertz O., Teyssier R., Moore B., 2011, MNRAS, 410, 1391
Allen S. W., Schmidt R. W., Fabian A. C., 2001, MNRAS, 328, L37
Anderson M. E., Bregman J. N., 2011, ApJ, 737, 22
Barton E. J., Cooke J., 2009, AJ, 138, 1817
Binney J., Nipoti C., Fraternali F., 2009, MNRAS, 397, 1804
Bowen D. V., Blades J. C., Pettini M., 1996, ApJ, 464, 141

Brook C. B., Governato F., Roškar R., Stinson G., Brooks A. M., Wadsley J., Quinn T., Gibson B. K., Snaith O., Pilkington K., House E., Pontzen A., 2011, MNRAS, 415, 1051

Brook C. B., Stinson G., Gibson B. K., Roškar R., Wadsley J., Quinn T., 2012, MNRAS, 419, 771

Brook C. B., Stinson G., Gibson B. K., Wadsley J., Quinn T., 2012, MNRAS accepted, ArXiv e-prints

Cen R., 2012, ApJ, 753, 17

Cen R., Ostriker J. P., 2006, ApJ, 650, 560

Chabrier G., 2003, PASP, 115, 763

Chen H.-W., Lanzetta K. M., 2003, ApJ, 597, 706

Chen H.-W., Tinker J. L., 2008, ApJ, 687, 745

Conroy C., Wechsler R. H., 2009, ApJ, 696, 620

Danforth C. W., Shull J. M., 2008, ApJ, 679, 194

Davé R., Oppenheimer B. D., Katz N., Kollmeier J. A., Weinberg D. H., 2010, MNRAS, 408, 2051

Ferland G. J., Korista K. T., Verner D. A., Ferguson J. W., Kingdon J. B., Verner E. M., 1998, PASP, 110, 761

Freyer T., Hensler G., Yorke H. W., 2006, ApJ, 638, 262

Fumagalli M., Prochaska J. X., Kasen D., Dekel A., Ceverino D., Primack J. R., 2012, MNRAS, 420, 1796

Gibson B. K., Giroux M. L., Penton S. V., Putman M. E., Stocke J. T., Shull J. M., 2000, AJ, 120, 1830

Gibson B. K., Giroux M. L., Penton S. V., Stocke J. T., Shull J. M., Tumlinson J., 2001, AJ, 122, 3280

Guo Q., White S., Boylan-Kolchin M., De Lucia G., Kauffmann G., Lemson G., Li C., Springel V., Weinmann S., 2011, MNRAS, 413, 101

Guo Q., White S., Li C., Boylan-Kolchin M., 2010, MNRAS, 404, 1111

Haardt F., Madau P., 2012, ApJ, 746, 125

Katz N., 1992, ApJ, 391, 502

Kaufmann T., Bullock J. S., Maller A. H., Fang T., Wadsley J., 2009, MNRAS, 396, 191

Kawata D., Rauch M., 2007, ApJ, 663, 38

Kereš D., Hernquist L., 2009, ApJ, 700, L1

Knollmann S. R., Knebe A., 2009, ApJS, 182, 608

Kroupa P., Tout C. A., Gilmore G., 1993, MNRAS, 262, 545

Lanzetta K. M., Wolfe A. M., Turnshek D. A., 1995, ApJ, 440, 435

Macciò A. V., Stinson G., Brook C. B., Wadsley J., Couchman H. M. P., Shen S., Gibson B. K., Quinn T., 2012, ApJ, 744, L9

Maller A. H., Bullock J. S., 2004, MNRAS, 355, 694

Mandelbaum R., Li C., Kauffmann G., White S. D. M., 2009, MNRAS, 393, 377

Mo H. J., Miralda-Escude J., 1996, ApJ, 469, 589

More S., van den Bosch F. C., Cacciato M., Skibba R., Mo H. J., Yang X., 2011, MNRAS, 410, 210

Moster B. P., Somerville R. S., Maulbetsch C., van den Bosch F. C., Macciò A. V., Naab T., Oser L., 2010, ApJ, 710, 903

Murray N., Ménard B., Thompson T. A., 2011, ApJ, 735, 66

Nath B. B., Silk J., 2009, MNRAS, 396, L90

Navarro J. F., Frenk C. S., White S. D. M., 1995, MNRAS, 275, 720

Oppenheimer B. D., Davé R., 2009, MNRAS, 395, 1875

Oppenheimer B. D., Davé R., Katz N., Kollmeier J. A., Weinberg D. H., 2012, MNRAS, 420, 820

Prochaska J. X., Weiner B., Chen H.-W., Mulchaey J., Cooksey K., 2011, ApJ, 740, 91

Rubin K. H. R., Prochaska J. X., Koo D. C., Phillips A. C., 2012, ApJ, 747, 26

Rubin K. H. R., Prochaska J. X., Koo D. C., Phillips A. C., Weiner B. J., 2010, ApJ, 712, 574

Rubin K. H. R., Weiner B. J., Koo D. C., Martin C. L., Prochaska J. X., Coil A. L., Newman J. A., 2010, ApJ, 719, 1503

Savage B. D., Lehner N., Narayanan A., 2011a, ApJ, 743, 180

Savage B. D., Narayanan A., Lehner N., Wakker B. P., 2011b, ApJ, 731, 14

Scannapieco C., Wadepuhl M., Parry O. H., Navarro J. F., Jenkins A., Springel V., Teyssier R., Carlson E., Couchman H. M. P., Crain R. A., 2012, MNRAS, 423, 1726

Sembach K. R., Wakker B. P., Savage B. D., Richter P., Meade M., Shull J. M., Jenkins E. B., Sonneborn G., Moos H. W., 2003, ApJS, 146, 165

Shapley A. E., Steidel C. C., Pettini M., Adelberger K. L., 2003, ApJ, 588, 65

Shen S., Madau P., Aguirre A., Guedes J., Mayer L., Wadsley J., 2011, ArXiv e-prints

Shen S., Wadsley J., Stinson G., 2010, MNRAS, 407, 1581

Smith B. D., Hallman E. J., Shull J. M., O'Shea B. W., 2011, ApJ, 731, 6

Springel V., 2010, MNRAS, 401, 791

Steidel C. C., Erb D. K., Shapley A. E., Pettini M., Reddy N., Bogosavljević M., Rudie G. C., Rakic O., 2010, ApJ, 717, 289

Stewart K. R., Kaufmann T., Bullock J. S., Barton E. J., Maller A. H., Diemand J., Wadsley J., 2011, ApJ, 738, 39

Stinson G., Seth A., Katz N., Wadsley J., Governato F., Quinn T., 2006, MNRAS, 373, 1074

Stinson G. S., Bailin J., Couchman H., Wadsley J., Shen S., Nickerson S., Brook C., Quinn T., 2010, MNRAS, 408, 812

Stocke J. T., Penton S. V., Danforth C. W., Shull J. M., Tumlinson J., McLin K. M., 2006, ApJ, 641, 217

Strickland D. K., Heckman T. M., Colbert E. J. M., Hoopes C. G., Weaver K. A., 2004, ApJ, 606, 829

Telfer R. C., Kriss G. A., Zheng W., Davidsen A. F., Tytler D., 2002, ApJ, 579, 500

Teyssier R., 2002, A&A, 385, 337

Thom C., Chen H.-W., 2008a, ApJS, 179, 37

Thom C., Chen H.-W., 2008b, ApJ, 683, 22

Thom C., Putman M. E., Gibson B. K., Christlieb N., Flynn C., Beers T. C., Wilhelm R., Lee Y. S., 2006, ApJ, 638, L97

Tripp T. M., Sembach K. R., Bowen D. V., Savage B. D., Jenkins E. B., Lehner N., Richter P., 2008, ApJS, 177, 39

Tumlinson J., Thom C., Werk J. K., Prochaska J. X., Tripp T. M., Weinberg D. H., Peeples M. S., O'Meara J. M., Oppenheimer B. D., Meiring J. D., Katz N. S., Dave R., Brady Ford A., Sembach K. R., 2011, Science, 334, 948

Vogelsberger M., Sijacki D., Keres D., Springel V., Hernquist L., 2011, ArXiv e-prints

Wadsley J. W., Stadel J., Quinn T., 2004, New Astronomy, 9, 137

Wakker B. P., Savage B. D., 2009, ApJS, 182, 378

Wakker B. P., Savage B. D., Fox A. J., Benjamin R. A., 2012, ApJ, 749, 157

Wakker B. P., van Woerden H., 1997, ARAA, 35, 217

Weiner B. J., Coil A. L., Prochaska J. X., Newman J. A., Cooper M. C., Bundy K., Conselice C. J., Dutton A. A., Faber S. M., Koo D. C., Lotz J. M., Rieke G. H., Rubin K. H. R., 2009, ApJ, 692, 187